# Minimum Detectability and Dose Analysis for Size-based Optimization of CT Protocols

by

Christopher Craig Smitherman

Graduate Program in Medical Physics
Duke University

Date:_____

Approved:

_____
Ehsan Samei, Supervisor

_____
Paul Segars

_____
James Bowsher

_____
Tracy Jaffe

Thesis submitted in partial fulfillment of
the requirements for the degree of
Master of Science in the Graduate Program in Medical Physics
in the Graduate School
of Duke University

2014

ABSTRACT

Minimum Detectability and Dose Analysis for Size-based Optimization of CT Protocols

by

Christopher Craig Smitherman

Graduate Program in Medical Physics
Duke University

Date:_____

Approved:

_____
Ehsan Samei, Supervisor

_____
Paul Segars

_____
James Bowsher

_____
Tracy Jaffe

An abstract of a thesis submitted in partial
fulfillment of the requirements for the degree
of Master of Science in the Graduate Program in Medical Physics
in the Graduate School of
Duke University

2014

# Abstract

**Purpose:** To develop a comprehensive model of task-based performance of CT across a broad library of CT protocols, so that radiation dose and image quality can be optimized within a large multi-vendor clinical facility.

**Methods:** 80 adult CT protocols from the Duke University Medical Center were grouped into 23 protocol groups with similar acquisition characteristics. A size-based image quality phantom (Duke Mercury Phantom 2.0) was imaged using these protocol groups for a range of clinically relevant dose levels on two CT manufacturer platforms (Siemens SOMATOM Definition Flash and GE CT750 HD). For each protocol group, phantom size, and dose level, the images were analyzed to extract task-based image quality metrics, the task transfer function (TTF) and the noise power spectrum (NPS). The TTF and NPS were further combined with generalized models of lesion task functions to predict the detectability of the lesions in terms of areas under the receiver operating characteristic curve ($A_z$). A graphical user interface (GUI) was developed to present $A_z$ as a function of lesion size and contrast, dose, patient size, and protocol, as well as to derive the necessary dose to achieve a detection threshold for a targeted lesion.

**Results:** The GUI provided the prediction of $A_z$ values modeling detection confidence for a targeted lesion, patient size, and dose. As an example, an abdomen pelvis exam for the GE scanner, with a task size/contrast of 5-mm/50-HU, and an $A_z$ of 0.9 indicated a

dose requirement of 4.0, 8.9, and 16.9 mGy for patient diameters of 25, 30, and 35 cm, respectively. For a constant patient diameter of 30 cm and 50-HU lesion contrast, the minimum detected lesion size at those dose levels were predicted to be 8.4, 5.0, and 3.9 mm, respectively.

**Conclusions:** A CT protocol optimization platform was developed by combining task-based detectability calculations with a GUI that demonstrates the tradeoff between dose and image quality. The platform can be used to improve individual protocol dose efficiency, as well as to improve protocol consistency across various patient diameters and CT scanners. The GUI can further be used to calculate personalized dose for individualized examination tasks.

# Contents

# List of Tables

# List of Figures

# 1. INTRODUCTION

Radiation exposure to the public has increased dramatically over the past decade with a majority of this increase being directly correlated to the increased utilization of computed tomography. Since increased radiation dose may increase the risk of cancer[1] [2] , the risks associated with CT are gaining national exposure from popular media outlets such as the New York Times and National Public Radio[3, 4], which raises alertness and anxiety among the patient population. Therefore, it is the responsibility of medical physicists in concert with radiologists and technologists to follow the ALARA (as low as reasonably achievable) mandate [5], to minimize radiation dose and reduce the risk to patients. A necessary requirement to implement ALARA is to optimize CT protocols, to lower the radiation dose as much as possible while maintaining adequate image quality for targeted diagnosis by the clinician.

Much has been done in the past to optimize CT protocols. The National Dose Index Registry [6] enables one to ensure dose appropriateness by comparing the dose delivered to a patient to those in the national registry. Individual technical factors making up the CT protocols have also been characterized to understand the effect each has on image quality and patient dose.[7] Observer studies have been conducted, where dose was reduced, mainly through tube current reduction, to compare the effects of dose reduction on radiologist diagnosis performance.[8] Zarb et al used phantom imaging to systematically optimize three protocols in terms of noise, low contrast visibility, and

resolution.[9] These optimized protocols were then subjectively evaluated in bovine CT images, bovine anatomy properties being similar to those of humans.[8] Larson et al used a predictive modeling of image noise to prospectively predict image quality to optimize chest abdomen pelvis protocols for radiation dose including the effect of patient size. [10, 11]

While the select studies highlighted above provide a strategy for optimizing CT protocols, they often focus on a very limited set of protocols and use incomplete image quality metrics. Meanwhile, clinical practice remains largely subjective and ad hoc, lacking scientific basis for the protocols employed. For example, most of the current practices have not effectively addressed the following questions: What is the appropriate dose reduction? How does one quantify the effect on image quality of a particular indication due to a specific decrease in dose? How do scanners from different vendors compare when it comes to dose-image quality trade off? How can a large radiology practice decide on appropriate image quality with differences in opinion and years of experience among radiologists? There is a need for a scientifically robust methodology for protocol optimization that is linked to radiologist detection confidence. Such a methodology can then aim to minimize radiation dose while providing consistent image quality across large, multi-vendor CT departments.

In this work, a comprehensive, systematic framework of task-based protocol optimization was developed, which aimed to evaluate and optimize the tradeoff

between image quality and radiation dose. The image quality was assessed with an image quality phantom and existing methodologies, which link image quality to radiologist detection confidence for combinations of protocols, patient sizes, dose levels, and lesions sizes and contrasts. The framework was designed to enable optimizing an extensive selection of CT protocols across a large academic medical center in a consistent and manageable fashion. It is envisioned that the strategy can be used as a first-step solid basis to target particular physical performance levels, which can further and subsequently be fine-tuned for clinical optimality.

# 2. METHODS AND MATERIALS

## *2.1 Image Quality Analysis*

To optimize CT protocols, the image quality was first assessed using an image quality phantom (Mercury phantom 2.0, Duke University Medical Center). [12] The Mercury phantom includes four cylindrical sections of increasing diameters (16, 23, 30, 37 cm), which are connected with tapered sections. [12] Each of the four sections includes four rod inserts of various HU (polystyrene, -40 HU; acrylic, 115 HU; Teflon, 910 HU; air, -1000 HU) which are used to measure contrast and the image resolution properties, as well as a uniformity section used to measure the image noise properties. [12] The resolution property is calculated in terms of a task transfer function (TTF) and the noise property in terms of a noise power spectrum (NPS), both using established methodologies, detailed in earlier publications. [13-15] The TTF and NPS can be combined with the task function, $W_{task}$ [13-15], the eye filter, E [16], and an internal noise, $N_i$ [16], to calculate the task-based observer performance in terms of a detectability index, d', as [15]

$$d'^2 = \frac{\left[\int\int TTF^2(u,v)\cdot E(u,v)^2\cdot\left|W_{task}(u,v)\right|^2 du\,dv\right]^2}{\int\int[NPS(u,v)+N_i(u,v)]\cdot TTF^2(u,v)\cdot E(u,v)^4\cdot\left|W_{task}(u,v)\right|^2 du\,dv}, \quad (1)$$

where u and v are the orthogonal spatial frequencies.

The numerator of the d' equation represents the signal while the denominator represents the distractions to the visualization of the signal. $W_{task}$ defines the contrast, shape, and size of the lesion that is targeted by the diagnostic task. In this work, the contrast and size (diameter) of the task was chosen to represent typical lesion sizes seen in the clinic. One hundred task functions having a range of contrast from 0.1 to 100 HU and a range of size from 0.1 to 15 mm were used. E modeled the spatial frequency response of the observer. An observer viewing distance of 50 cm was used in this study. [17] $N_i$ models the internal noise of the observer during the perception process. [15] Assuming Gaussian statistics, the d' was converted into the area under the receiver operating characteristic curve, $A_z$, as [18]

$$d' = 2 * erf^{-1}(2 * A_z - 1). \quad (2)$$

## *2.2 Protocol Organization*

A total of 80 protocols from Duke University Medical Center were selected for this study, including 38 for the Siemens Healthcare SOMATOM Definition Flash scanner (Germany) and 42 for the GE Healthcare CT750 HD scanner (Waukesha, WI) as shown in Table 1. The protocols chosen were developed for the abdominal ("body"), neurological ("neuro"), thoracic ("chest") and cardiovascular ("CVI") examinations (research scan protocols were excluded). Based on the 80 protocols, protocols of the same body type and consisting of the same technical factors, such as slice thickness, noise index/quality reference mAs, kernel, etc, were grouped together into so called

"super protocols." [Table 2]These super protocols were possible because much of the differences in clinical protocols were due to the timing of contrast and scan regions and not the difference in technical factors.

**Table 1: Grouping of protocols into super protocols.**

| Super Protocol | Siemens | GE |
|---|---|---|
| AP | AP | AP |
| | Adrenal | Cirrhosis |
| | CAP | Genitourinary |
| | Cholangiocarcinoma | Renal Donor |
| | Cirrhosis | Transitional Cell Carcinoma |
| | Dual Liver | Volume of Liver and Spleen |
| | Genitourinary | Adrenal |
| | Hepatic Resection | Cystogram |
| | Focused Renal Cyst | Hepatic Resection |
| | Renal Cell Carcinoma | Mesenteric Ischemia |
| | CTA Renal Donor | Trauma AP |
| | Crohns Disease | Radio-embolization |
| | Mesenteric Ischemia | CAP |
| | Occult GI Bleed | Dual Liver |
| | Transitional Cell Carcinoma | Focused Renal Cyst |
| | Trauma AP | Crohns Disease |
| | Trauma CAP | Trauma CAP |
| | Valsalva AP | Cholangio-carcinoma |
| | Volume of Liver and Spleen | Dual Pancreas |
| | Radioembolization | Renal Cell Carcinoma |
| | Renal Stone | Occult GI Bleed |
| | | Valsalva AP |
| Renal stone | N/A | Renal Stone |
| Brain | Adults Brain | Adult Brain |
| Brain 0 to 3 | N/A | Ped Brain 0 to 3 |
| Brain 4 to 7 | N/A | Ped Brain 4 to 7 |
| Brain 0 to 5 | Ped Brain 0-5 | N/A |
| CTA COW | CTA Circle of Willis | CTA Circle of Willis |
| CTA Carotid | CTA Carotid | CTA Carotid |
| | CTA Combo | CTA Combo |
| Neck | Neck | Neck |
| Face | Sinus | Sinus |
| | Face | Face |

| | | |
|---|---|---|
| | Orbits | Orbits |
| Standard Chest | Standard Chest<br>Follow up ILD<br>Airway<br>New ILD<br>BOS Chest<br>Bronchiectasis | Standard Chest |
| Low Dose Chest | Low dose chest | Chest Screening<br>Low Dose Chest<br>Airway |
| Hi Res Chest | N/A | Mesothelioma<br>Bronchiectasis<br>New ILD<br>Follow Up ILD |
| PE Chest | PE Chest | PE Chest |

**Table 2: Technical factors of the super protocols for the Siemens Flash (a) and GE 750HD (b) scanner.**

**a)**

| | **kVp** | **Quality Reference mAs** | **Scan Mode** | **Reconstruction Algorithm** | **Kernel** | **Slice Thickness** | **Slice Interval** |
|---|---|---|---|---|---|---|---|
| **AP** | 120 | 200 | Helical | SAFIRE 2[1] | i31 | 5 mm | 5 mm |
| **Brain** | 120 | 285 | Helical | SAFIRE 2 | j45s | 5 mm | 1 mm |
| **Brain 0-5** | 120 | 80 | Helical | SAFIRE 2 | j45s | 5 mm | 1 mm |
| **CTA COW** | 120 | 285 | Helical | SAFIRE 2 | i30 | 0.75 mm | 0.7 mm |
| **CTA Carotid** | 120 | 300 | Helical | SAFIRE 2 | i30 | 0.75 mm | 0.7 mm |
| **Neck** | 120 | 200 | Helical | SAFIRE 2 | i31 | 2 mm | 2 mm |
| **Face** | 120 | 200 | Helical | SAFIRE 2 | i31 | 2 mm | 2 mm |
| **Standard Chest** | 120 | 150 | Helical | FBP | B31f | 5 mm | 5 mm |
| **Low Dose** | 120 | 100 | Helical | FBP | B31f | 5 mm | 5 mm |
| **PE** | 120 | 250 | Helical | FBP | B30f | 1 mm | 1 mm |

**b)**

| | kVp | Noise Index or mAs | Scan Mode | Reconstruction Algorithm | Kernel | Slice Thickness | Slice Interval |
|---|---|---|---|---|---|---|---|
| **AP** | 120 | NI = 22 | Helical | ASIR 40%[2] | Standard | 5 mm | 5 mm |
| **Renal Stone** | 120 | NI = 25 | Helical | ASIR 40% | Standard | 5 mm | 5 mm |
| **Brain** | 120 | mAs = 335 | Axial | ASIR 40% | Standard | 5 mm/4i | 20 mm |
| **Brain 0 to 3** | 120 | mAs = 105 | Axial | ASIR 40% | Standard | 5 mm/4i | 20 mm |
| **Brain 4 to 7** | 120 | mAs = 155 | Axial | ASIR 40% | Standard | 5 mm/4i | 20 mm |
| **CTA COW** | 120 | NI = 10 | Helical | ASIR 40% | Soft | 0.625 mm | 0.625 mm |
| **CTA Carotid** | 120 | NI = 13 | Helical | ASIR 40% | Soft | 0.625 mm | 0.625 mm |
| **Neck** | 120 | NI = 10 | Helical | ASIR 40% | Standard | 2.5 mm | 2.5 mm |
| **Face** | 120 | mAs = 335 | Axial | ASIR 40% | Standard | 2.5 mm/8i | 20 mm |
| **Standard Chest** | 120 | NI = 19.2 | Helical | ASIR 30% | Standard | 5 mm | 5 mm |
| **Low Dose Chest** | 120 | NI = 30 | Helical | ASIR 30% | Standard | 5 mm | 5 mm |
| **Hi Res Chest** | 120 | NI = 13.8 | Helical | ASIR 30% | Standard | 5 mm | 5 mm |
| **PE** | 120 | NI = 12 | Helical | ASIR 30% | Standard | 5 mm | 5 mm |

1. 1. SAFIRE 2 is Siemens Healthcare's iterative reconstruction (Sinogram Affirmed Iterative Reconstruction) with strength of 2.
2. ASIR 40% is GE Healthcare's iterative reconstruction (Adaptive Statistical Iterative Reconstruction). The percentage represents the percentage of iterative reconstruction of the total reconstruction. Remaining percentage uses FBP.

## *2.3 Data Acquisition and Processing*

The Mercury phantom was imaged using the protocols detailed above. The only difference between the protocols and the acquired scans was a change from automatic tube current modulation (TCM) in clinical procedures to a fixed tube current in the data acquisition. TCM is used in CT to adaptively adjust the x-ray flux to provide consistent image quality in terms of image noise across the imaging field. The noise index (GE) or quality reference mAs (Siemens) are scanner-specific technical factors used to define "targeted" noise levels in image acquisitions. A lower noise level (through a lower noise index or higher quality reference mAs) leads to a higher $CTDI_{vol}$, for the entire exam.

In this study, TCM was not used, as our goal was to use exam $CTDI_{vol}$ as the optimization target for an imaging examination. In doing so, we assumed that the relationship between $CTDI_{vol}$ (based on constant mAs) and image quality characterized for a constant-diameter section of the phantom would be largely representative of that for a patient that shares the same average cross sectional area. Using this assumption, any TCM setting that would yield the targeted optimized $CTDI_{vol}$ value, would also render the desired representative image quality from the patient.

For abdominal and thoracic protocols, four dose index values corresponding to the target $CTDI_{vol}$ for patient diameters of 25, 30, 35, and 40 cm were used to bracket typical clinical scan dose index levels. These existing target $CTDI_{vol}$ values were informed by clinical dose data from our dose monitoring program [19] and are used by

CT technologists to ensure appropriate dose delivery in clinical studies. Imaging the phantom at these four dose index levels provided the images at the targeted dose index level and at three additional dose index levels for each diameter of the phantom to characterize image quality as a function of dose index. For "neuro" protocols (scans of the brain, face and neck), the patient thickness does not vary drastically in adults so there was only one target $CTDI_{vol}$ value in the protocols, but two additional dose index levels at approximately half and double the target $CTDI_{vol}$ were also used.

For each acquisition associated with a super protocol, the manual mA settings were adjusted to achieve the desired $CTDI_{vol}$ values on both scanners. Each dataset was reconstructed with reconstruction field of views of 18, 25, 32 and 39 cm (consistent with the section size being reconstructed), allowing 1 cm gap on either side of each section of the Mercury phantom. The data were then processed to extract the TTF, the NPS, and d' and corresponding $A_z$ for the targeted lesions for each combination of super-protocol, section diameter, dose index level, and reconstruction field of view amounting to over 100,000 values for each metric.

## *2.4 Graphical User Interface*

To facilitate data analytics, first, a graphical user interface (GUI) [Figure 1] was created using MATLAB (Mathworks) to simplify the presentation of the detectability data so that a large library of protocols could be evaluated in a user-friendly environment.

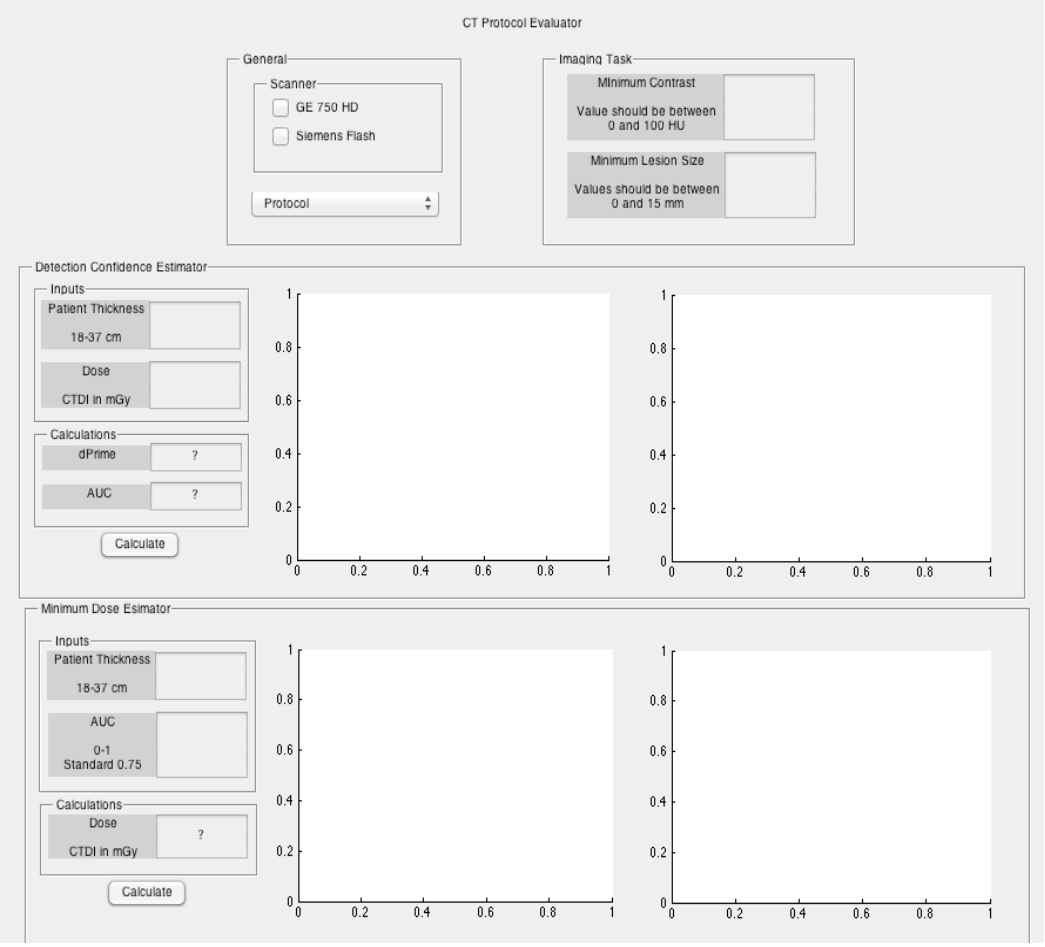


**Figure 1: Blank representation of CT Protocol Evaluation Platform. Blank boxes are user inputs while the boxes containing question marks are be calculated by the interface.**

To optimize a protocol, the user would first select the scanner for evaluation using a check box, which populates the protocol dropdown menu for the protocols corresponding to the selected scanner. These protocols are linked to the d' files corresponding to the appropriate super-protocol. Next, the user would input the lesion contrast and size that will be used in the calculation sections of the GUI. [Figure 2] This

lesion contrast and size reflect the detection threshold since lesions with greater values will be readily discernable. Similarly, the dose index calculated for the "minimum" entered lesion contrast and size can be characterized as the minimum necessary dose index since it represents the lowest dose index to detect the inputted lesion with the appropriate inputted detection confidence.

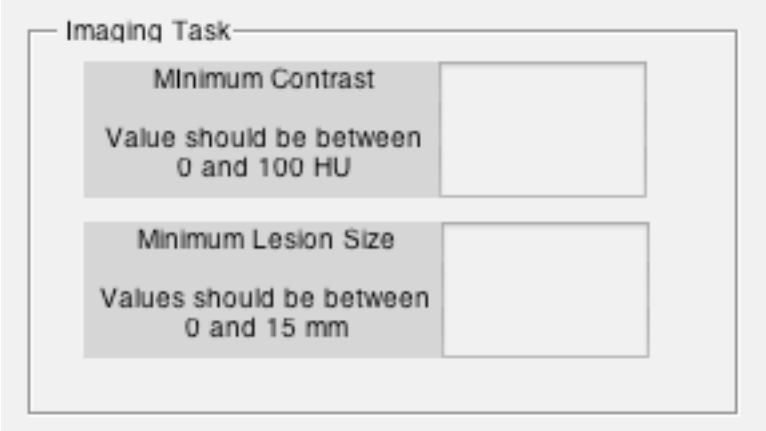


**Figure 2: User input to define the Task Function. The top box represents the task contrast value and should be between 0 and 100 HU. The bottom box represents the task size and should be between 0 and 15 mm.**

The GUI contains two sections that can be used to calculate the detectability or the minimum necessary dose index, respectively. In the first calculation section, the detection confidence section, the user inputs a patient diameter (between 18 and 37 cm) and a clinically relevant dose index (mGy) for evaluation. The d' and corresponding $A_z$ are calculated for the inputted task function characteristics, patient diameter, and dose index. In the minimum dose estimator section, the user inputs a patient diameter

(between 18 and 37 cm) and an $A_z$ value for evaluation. The program then calculates the minimum necessary dose index for the detectability of the inputted task function with the inputted detection confidence ($A_z$) for the inputted patient diameter.

## *2.5 Utilization of Platform*

A characterization of the platform was performed to see how the calculated detectability indices behave as a function of $CTDI_{vol}$, patient size, lesion size, and lesion contrast. Functional trends were ascertained to verify expected behavior and to explore the utility of the platform.

The GUI was designed to be used as an optimization tool for CT protocols in terms of image quality and dose. To demonstrate this, first the detectability index and corresponding $A_z$ were calculated for a 25, 30, and 35 cm cross-sectional diameter, a reference lesion size of 5 mm and contrast of 50 HU, and the abdomen pelvis protocol for the GE 750 HD, using the current clinical target dose index values. Furthermore, $CTDI_{vol}$ values for the three sizes and the reference imaging task were calculated to achieve an $A_z$ of 0.8. Using the three calculated $CTDI_{vol}$ values, the minimum size lesion was further calculated for a patient size of 30 cm.

A similar demonstration was completed to show how the platform could be used to compare image quality and dose across vendors for the same protocol. Using a 5 mm/50 HU lesion, $CTDI_{vol}$ was calculated for 25, 30, and 35 cm patients to achieve an $A_z$ of 0.85 for the standard chest protocol for both the GE 750 HD and Siemens Flash.

As a demonstration of the utility of the platform across the entire library of protocols, the platform was used to calculate the minimum necessary $CTDI_{vol}$ to detect the reference lesion in a clinically appropriate patient diameter with an observer detectability confidence ($A_z$) of 0.9 in all super protocols for both the GE 750 HD and the Siemens Flash scanners. A phantom containing low contrast lesions was further used to subjectively evaluate the $A_z$ prediction of the program. The phantom, designed as a supplement to the next version of Mercury phantom (Mercury 3.0), had inserts of various low-contrast and size to visually validate predicted detectability. [20]

# 3. Results

## *3.1 Graphical User Interface Functions*

To demonstrate the detectability index and corresponding $A_z$ for the specific combination of user inputs, the example below shows that for an abdomen pelvis protocol for the GE scanner, a patient size of 30 cm and a $CTDI_{vol}$ of 8, the GUI calculated the detectability index of 1.7 and corresponding $A_z$ of 0.88 for a 5 mm/50 HU lesion. In Figure 3, the plot on the left represents the calculated $A_z$ (green line), an $A_z = 0.6$ (red line), and an $A_z = 0.95$ (blue line) trend as a function of lesion size and patient thickness. The plot on the right represents the calculated $A_z$ (green line), an $A_z = 0.6$ (red line), and an $A_z = 0.95$ (blue line) trend as a function of task size and contrast.

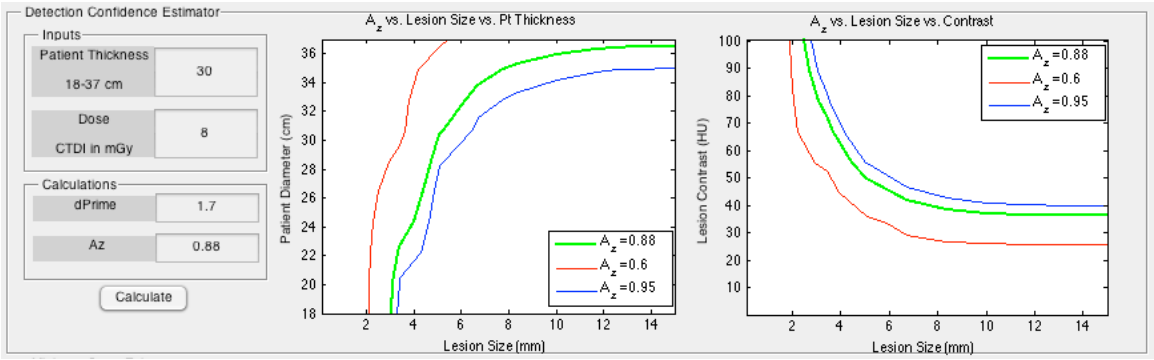


**Figure 3: Example of the detection confidence section of the CT protocol evaluator platform.**

As a demonstration on how the minimum necessary dose index may be determined for a specific combination of user inputs, an example for an abdomen pelvis protocol for the GE scanner show the calculated necessary $CTDI_{vol}$ of 8.88 to achieve an

$A_z$ of 0.9 for a 5 mm/50 HU lesion. In Figure 4, the plot on the left represents the calculated dose index (green line), a higher dose index (red line), and a lower dose index (blue line) detectability trend as a function of lesion size and patient diameter. The plot on the right represents the calculated dose index (green line), a higher dose index (red line), and a lower dose index (blue line) detectability trend as a function of lesion size and lesion contrast.

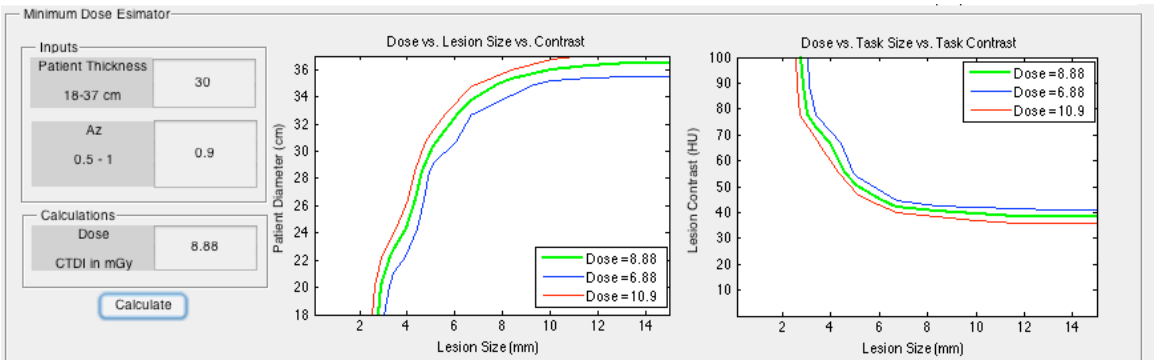


**Figure 4: Example of the minimum dose estimator section of the CT protocol evaluator platform.**

## *3.2 Data Trend Analysis*

As noted above, d' values were calculated for 100 tasks (task contrast ranging from 0 to 100 HU and task size ranging from 0 to 15 mm) with respect to protocol, dose index level, and section diameter. Table 3 shows the calculated d' values for a 30 cm patient diameter, abdomen pelvis exam, and 8 mGy $CTDI_{vol}$ on the GE scanner. The results show expected trends as the detectability index increases with increasing task size and contrast.

**Table 3: Example of table of d′ showing the effect of task contrast (HU) and task size (mm).**

| | | Task Size (mm) | | | | | | | | | |
|---|---|---|---|---|---|---|---|---|---|---|---|
| | | **0.1** | **1.8** | **3.4** | **5.1** | **6.7** | **8.4** | **10.0** | **11.7** | **13.3** | **15.0** |
| **Task Contrast (HU)** | **0** | 0 | 0 | 0 | 0 | 0 | 0 | 0 | 0 | 0 | 0 |
| | **11** | 0 | 0 | 0 | 0 | 0 | 0 | 0 | 0 | 0 | 0 |
| | **22** | 0 | 0 | 0 | 0 | 0 | 0 | 0 | 0 | 0 | 0 |
| | **33** | 0 | 0 | 0 | 0.1 | .06 | 0.9 | .11 | 1.2 | 1.2 | 1.2 |
| | **45** | 0 | 0 | 0 | 1.1 | 2.0 | 2.6 | 2.9 | 3.1 | 3.1 | 3.1 |
| | **56** | 0 | 0 | 0.5 | 2.4 | 3.7 | 4.6 | 5.1 | 5.4 | 5.5 | 5.6 |
| | **67** | 0 | 0 | 1.3 | 3.7 | 5.5 | 6.8 | 7.6 | 8.0 | 8.3 | 8.3 |
| | **78** | 0 | 0 | 2.1 | 5.1 | 7.4 | 9.1 | 10.2 | 10.9 | 11.3 | 11.5 |
| | **89** | 0 | 0 | 3.0 | 6.6 | 9.3 | 11.5 | 13.0 | 13.9 | 14.5 | 14.8 |
| | **100** | 0 | 0 | 3.9 | 8.0 | 11.3 | 13.9 | 15.9 | 17.1 | 17.9 | 18.4 |

Detectability is directly proportional to radiation dose and indirectly proportional to patient diameter. Figure 5 verifies these trends by analyzing an abdomen pelvis protocol on the GE scanner with increasing dose index and patient diameter. The plots in Figure 5 represent $A_z$ values. A shift towards the origin represents an increase in detectability because lower contrast and smaller lesion are detectable. The $A_z$ plots shift away from origin when moving from left to right representing decreased

detectability due to increased patient thickness. Moving from bottom to top, the $A_z$ plots shift toward the origin to represent increased detectability with increasing dose index.

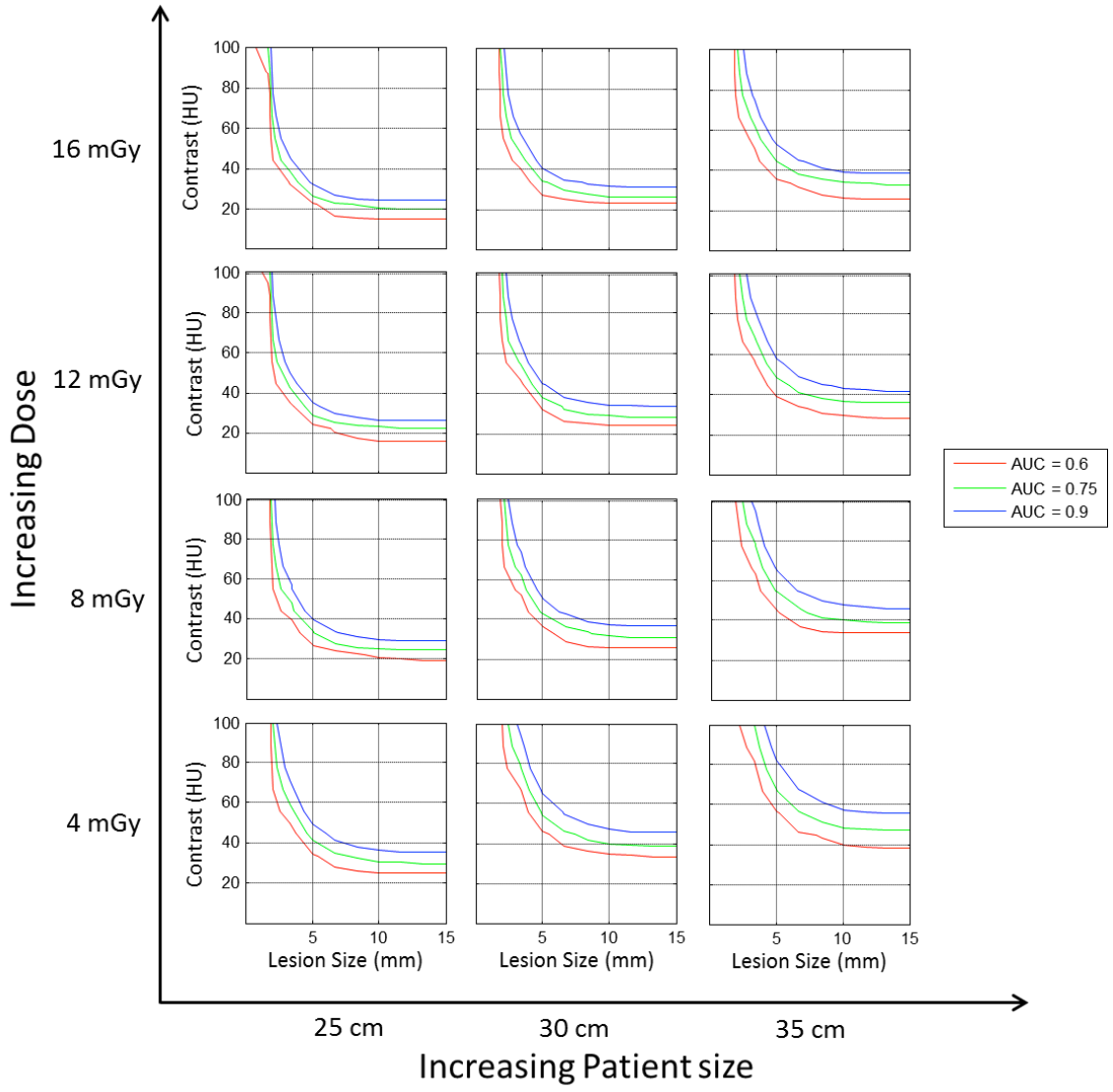


**Figure 5: Detectability trend analysis showing the effects of patient diameter and dose index on detection confidence, $A_z$. The x-axis of the plots of the figure represents**

**mean contrast (HU) of task functions and the y-axis of the plots of the figure represents lesion size (mm) of the task functions.**

## *3.3 Protocol Optimization Demonstration*

Table 4 tabulates the calculated $CTDI_{vol}$ values for varying patient size. Table 5 further shows the minimum detectable lesion sizes for varying dose index levels with a fixed patient size. An abdomen pelvis exam for the GE 750 HD scanner using a task size/contrast of 5-mm/50-HU, and an $A_z$ of 0.9 was used for calculations. As shown in Table 4, $CTDI_{vol}$ must increase from 4.0 to 16.9 to maintain image quality with increasing patient size from 25 to 35 cm. As shown in Table 5, increasing $CTDI_{vol}$ from 4.0 to 16.9 mGy decreases the minimum detectable lesion size from 8.4 to 3.9 mm.

**Table 4: Effect of patient diameter on calculated necessary dose index for the GE 750HD abdomen pelvis protocol with an $A_z$ of 0.9, task contrast of 50 HU and task size of 5 mm.**

| Patient Diameter | Dose Index ($CTDI_{vol}$) |
|---|---|
| **25 cm** | 4.0 |
| **30 cm** | 8.9 |
| **35 cm** | 16.9 |

**Table 5: Effect of dose on the minimum lesion size detected for the GE 750HD abdomen pelvis protocol with a patient diameter of 30 cm, $A_z$ of 0.9, and task contrast of 50 HU.**

| Dose index | Minimum Lesion Size |
|---|---|
| **4.0 mGy** | 8.4 mm |
| **8.9 mGy** | 5.0 mm |
| **16.9 mGy** | 3.9 mm |

Using a task function of 50 HU contrast and 5 mm size, Columns 3 and 4 of Table 6 lists the minimum detectability and $A_z$ value when using the appropriate target $CTDI_{vol}$ for the respective patient diameters. Currently in the clinic, CT technologist use target $CTDI_{vol}$ values for select patient sizes to ensure that the dose during imaging exams is appropriate. As noted earlier, these values were gathered using the Duke dose-monitoring program. The CT protocol evaluation platform was used to calculate appropriate dose index levels to ensure consistent image quality across patient diameters, as shown in Column 5 of Table 6.

**Table 6: Minimum detectability analysis using the existing target doses for the abdomen pelvis protocol on the GE 750HD scanner and comparison to the calculated necessary doses to achieve consistent image quality ($A_z$ = 0.8) across patient diameters.**

| Patient Diameter | Existing Target $CTDI_{vol}$ | Calculated d′ | Calculated $A_z$ | Calculated Necessary $CTDI_{vol}$ |
|---|---|---|---|---|
| **25 cm** | 4 | 1.9 | 0.91 | 4.0 |
| **30 cm** | 6 | 1.3 | 0.83 | 5.6 |
| **35 cm** | 10 | 0.82 | 0.72 | 13.5 |

Using the existing target dose index level for their respective patient diameters, the $A_z$ decreases by 9% from the 25 to 30 cm patient diameter and decreases by an additional 14% from the 30 to 35 cm patient diameter. The dose value calculated for the 25 cm patient diameter is equivalent to the existing value while the calculated minimum dose index for the 30 cm patient diameter is 1.04 mGy less than the existing value and the

calculated minimum dose index for the 35 cm patient diameter is 1.3 mGy higher than the existing value.

Table 7 shows the proposed dose index to achieve an $A_z$ of 0.85 for 25, 30, and 35 patient sizes for a 5 mm/50 HU lesion for the standard chest protocol for both the Siemens and GE scanners. Using these target $CTDI_{vol}$ values will achieve equivalent image quality for all patient diameters across vendors.

**Table 7: Minimum necessary $CTDI_{vol}$) comparison of the Siemens Flash and GE 750 HD for the standard chest protocol.**

| | Siemens | GE |
|---|---|---|
| **Patient Diameter** | Proposed Target Dose Index ($CTDI_{vol}$) | Proposed Target Dose Index ($CTDI_{vol}$) |
| **25** | 6.0 | 3.0 |
| **30** | 11.0 | 8.6 |
| **35** | 14.1 | 16.2 |

The minimum necessary dose index to detect a reference lesion (5 mm, 50 HU contrast for abdominal and neuro protocols; 5 mm, 60 HU contrast for chest protocols) in all super protocols for both scanners are listed in Table 8. Patient diameters of 25, 30 and 35 cm were used for the abdomen pelvis and standard chest protocols while a 25 cm patient diameter was used for neuro protocols.

**Table 8: Example minimum necessary dose index calculations using a reference lesion. N/A is used to reflect the differences in the naming of protocols between scanners.**

| Super Protocol | Siemens | | | GE | | |
|---|---|---|---|---|---|---|
| | **25 cm** | **30 cm** | **35 cm** | **25 cm** | **30 cm** | **35 cm** |
| **AP** | 6.08 | 6.51 | 9.74 | 3.96 | 8.88 | 16.9 |
| **Renal Stone** | N/A | N/A | N/A | 4.03 | 12.4 | 14.6 |
| **Brain** | 21.2 | N/A | N/A | 9.98 | N/A | N/A |
| **Brain 0 to 3** | N/A | N/A | N/A | 7.72 | N/A | N/A |
| **Brain 4 to 7** | N/A | N/A | N/A | 8.51 | N/A | N/A |
| **Brain 0 to 5** | 8.49 | N/A | N/A | N/A | N/A | N/A |
| **CTA COW** | 27.5 | N/A | N/A | 37.7 | N/A | N/A |
| **CTA Carotid** | 8.26 | N/A | N/A | 14.7 | N/A | N/A |
| **Neck** | 5.01 | N/A | N/A | 22.2 | N/A | N/A |
| **Face** | 9.42 | N/A | N/A | 15 | N/A | N/A |
| **Standard Chest** | 6 | 8.49 | 14.1 | 2 | 5.31 | 13.3 |
| **Low Dose Chest** | 4.05 | 7.64 | 10.1 | 2.2 | 6.64 | 11 |
| **Hi Res Chest** | N/A | N/A | N/A | 5.99 | 7.52 | 14.5 |
| **PE Chest** | 7.97 | 17.6 | 32.5 | 7.91 | 8.48 | 11.1 |

## *3.4 Low Contrast Phantom for Verification*

An image of a low contrast lesion phantom was used for subjective verification of the calculated values of the GUI. In Figure 6, the predicted $A_z$ value is superimposed on an image of the low contrast phantom. An $A_z$ of 0.65 was calculated for the displayed 0.6 mm/20 HU lesion insert. It is evident that the level of subtlety of the inserts are in general concert with the expected calculated $A_z$.

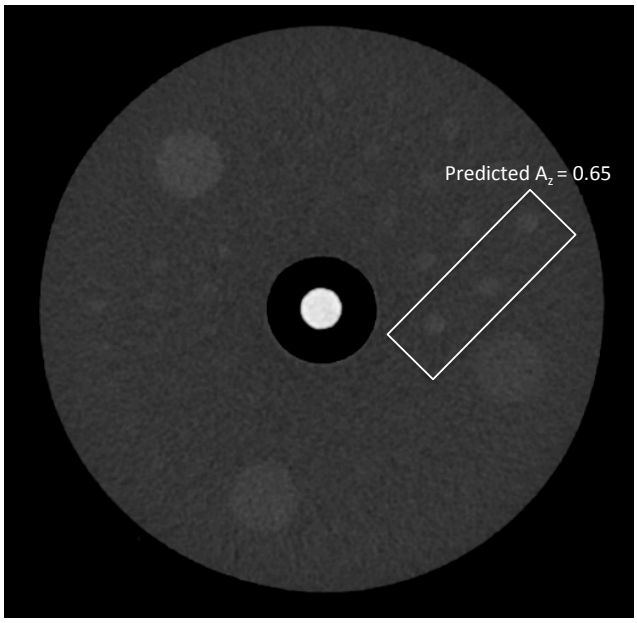


**Figure 6: Image of low contrast lesion phantom. An $A_z$ of 0.65 was predicted for the lesion inserts inside of the white box.**

# 4. Discussion

Due to the increase use of CT and its associated radiation risk, it is important to optimize CT protocols to reduce dose while maintaining adequate image quality. Protocol optimization currently utilized in the clinic is subjective and lacks scientific rigor. In this work, a systematic, scientific methodology linked to perception was created to optimize CT protocols. We objectively measured the image quality with a phantom [12] that had the ability to represent a range of patient sizes. The detectability index, d', a task based image quality metric, was used because of its ability to comprehensively incorporate contrast, resolution, and noise to model observer diagnostic performance. [21] Our task-based, size specific evaluation platform utilized image quality and radiation dose as the fundamental metrics of optimization. Using this process, it is possible to optimize, compare, and personalize CT protocol libraries at large multi-vendor departments.

This platform has three utilities to optimize the protocols of a CT department. First, it can be used to optimize the protocols for a single CT scanner so that the minimum dose is used for all patient sizes such that all image sets have generally consistent image quality. To do so, a typical task is entered into the task function section of the GUI as a starting point. If clinical CT protocols have current target dose levels for patient sizes, these values should be entered into the system individually to calculate the detectability and corresponding $A_z$ [Table 5]. For an optimum protocol giving consistent

image quality across all patient diameters, one may target the calculated $A_z$ values to be equivalent, representing an appropriate dose to all patient sizes to achieve the same detection confidence. This can be achieved by adjusting the dose levels for the specific patient diameters to achieve equivalent $A_z$ for all patient diameters. The method can similarly be used for individualizing examinations by optimizing the target $CTDI_{vol}$ for specific patient diameters. Using a typical clinical task for the protocol, the minimum dose index is calculated for specific patient diameters so CT technologists have appropriate dose index target values for a range of patient diameters. These calculated dose index values may be used to achieve target consistent image quality across all patient diameters.

The second utility of the CT evaluation platform is to optimize CT protocols by improving image quality consistency across multiple vendors. The scanners can be compared using both the detection confidence and the minimum necessary dose index analysis. In order to optimize image quality across vendors, an acceptable $A_z$ value for a typical task can be used to calculate the target dose index values for the specific patient diameters on each scanner. This would provide consistent image quality for all patient diameters and scanners aiming for all patients to be imaged at the same image quality at the lowest possible dose. A minimum dose analysis was done on for all super protocols to compare the two scanners. These results support the hypothesis of a large variability in the scanner and protocol performance in CT departments even when much work has

been done to optimize protocols. Multi-vendor radiology departments serve too many patients to funnel certain procedures to specific scanners in order to achieve better image quality with lower dose if one scanner is vastly outperforming another. Instead, this evaluation highlights the differences in scanners so that radiologists, medical physicists, and technologists can change technical factors in specific protocols during protocol review to level the performance between scanners. Further optimization can be achieved by defining an appropriate $A_z$ for a clinically relevant task to calculate the minimum necessary dose index for each patient diameter.

The third utility of the optimization platform is personalized dose calculations. In an optimal CT department, the protocol can be personalized for each patient so a minimum dose is received for appropriate $A_z$ for a specific task. As a demonstration, if a patient with 33 cm diameter presented with a clinical task with a contrast of 45 HU, a size of 4.5 mm, and the detection confidence needed was $A_z$=0.8 for accurate diagnosis, Figure 7 shows the calculation for minimum necessary dose index to achieve that goal.

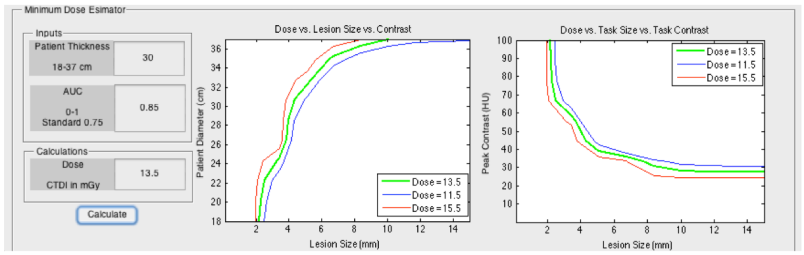


a)

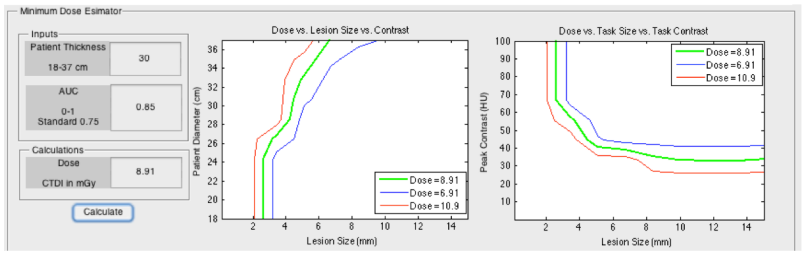


b)

**Figure 7: Personalized dose calculation for the GE 750HD (a) and the Siemens Flash (b).**

Notwithstanding the utility and the reach of the methodology, there are some limitations. First, this work does not use tube current modulation in its evaluation. It assumes an average dose and an average patient diameter to reasonably represent a CT examination. The manual doses used for the study reasonably bracket clinical ranges; however, additional studies will aid in devising possible accommodation for differences in the TCM algorithms. Secondly, this work was limited to the analysis of a single typical task for each calculation. If the task were unknown or if there were multiple tasks present, the case would be evaluated on a typical limiting task for the imaging study. Thirdly, this work was limited to only two commercial CT scanners. Additional makes and models should be incorporated in future studies. Finally, while a visual

inspection of a low-contrast phantom validates the general applicability of the results, a complete observer study is warranted to fully validate the generalizability of the approach. Nonetheless, the strategy pursued in this study provides a methodology for initial optimization of CT protocols with metrics more nuanced than the first order optimizations based on the CNR. This second-order strategy can be used as a precursor for further follow-up clinical fine-tuning.

# 5. Conclusion

This work has demonstrated a systematic approach to CT protocol optimization in terms of radiation dose index and image quality. The platform created could be used to approach image quality consistency across large multi-vendor departments with numerous protocol definitions. It provides a scientific basis for protocol optimization and benefits the patients and practitioners by maintaining targeted initial detection confidence at the lowest radiation dose.

# References


1. Brenner, D.J. and E.J. Hall, *Computed tomography--an increasing source of radiation exposure.* N Engl J Med, 2007. **357**(22): p. 2277-84.

2. Marin, D., et al., *Body CT: technical advances for improving safety.* AJR Am J Roentgenol, 2011. **197**(1): p. 33-41.

3. Brody, J.E. *Medical Radiation Soars, With Risks Often Overlooked*. The New York Times, 2012.

4. Knox, R. *Radiation From CT Scans May Raise Cancer Risk*. 2009.

5. *Part 20-Standard for Protection Against Radiation*. 2013 March 11, 2014 [cited 2014 March 27]; Available from: http://www.nrc.gov/reading-rm/doc-collections/cfr/part020/.

6. Kofler, J.M., D.D. Cody, and R.L. Morin, *CT Protocol Review and Optimization.* J Am Coll Radiol, 2014. **11**(3): p. 267-70.

7. Lambert, J., et al., *Techniques and Tactics for Optimizing CT Dose in Adults and Children: State of the Art and Future Advances.* J Am Coll Radiol, 2014. **11**(3): p. 262-6.

8. Kubo, T., et al., *Radiation dose reduction in chest CT: a review.* AJR Am J Roentgenol, 2008. **190**(2): p. 335-43.

9. Zarb, F., M.F. McEntee, and L. Rainford, *CT radiation dose and image quality optimization using a porcine model.* Radiol Technol, 2013. **85**(2): p. 127-36.

10. Larson, D.B., et al., *System for verifiable CT radiation dose optimization based on image quality. part II. process control system.* Radiology, 2013. **269**(1): p. 177-85.

11. Larson, D.B., et al., *System for verifiable CT radiation dose optimization based on image quality. part I. Optimization model.* Radiology, 2013. **269**(1): p. 167-76.

12. Wilson, J.M., et al., *A methodology for image quality evaluation of advanced CT systems.* Med Phys, 2013. **40**(3): p. 031908.

13. Chen, B., et al., *Volumetric quantification of lung nodules in CT with iterative reconstruction (ASiR and MBIR).* Med Phys, 2013. **40**(11): p. 111902.

14. Richard, S. and E. Samei, *Quantitative imaging in breast tomosynthesis and CT: comparison of detection and estimation task performance.* Med Phys, 2010. **37**(6): p. 2627-37.

15. Baiyu Chen, E.S., *Development of a phantom-based methodology for the assessment of quantification performance in CT*, in *Proc SPIE 8668*2013, Medical Imaging 2013: Physics of Medical Imaging: Lake Buena Vista Florida.

16. Burgess, A.E., *Visual perception studies and observer models in medical imaging.* Semin Nucl Med, 2011. **41**(6): p. 419-36.

17. Samei, E., M.J. Flynn, and W.R. Eyler, *Detection of subtle lung nodules: relative influence of quantum and anatomic noise on chest radiographs.* Radiology, 1999. **213**(3): p. 727-34.

18. Nghia Q. Ngyuen, e.a., *Detectability index describes the information conveyed by sonographic images.* Ultrasonics Symposium, 2011: p. 680 - 683.

19. Christianson, O., et al., *Automated size-specific CT dose monitoring program: assessing variability in CT dose.* Med Phys, 2012. **39**(11): p. 7131-9.

20. Justin Solomon, F.B., Ehsan Samei, *Design of anthropomorphic textured phantoms for CT performance evaluation*, in *Medical Imaging 2014: Physics of Medical Imaging*2014.

21. Gang, G.J., et al., *Analysis of Fourier-domain task-based detectability index in tomosynthesis and cone-beam CT in relation to human observer performance.* Med Phys, 2011. **38**(4): p. 1754-68.